Radiat Environ Biophys (2011) 50:281–297
DOI 10.1007/s00411-011-0357-x

ORIGINAL PAPER

Effect of site-specific bronchial radon progeny deposition on the spatial and temporal distributions of cellular responses

Árpád Farkas · Werner Hofmann · Imre Balásházy · István Szőke · Balázs G. Madas · Mona Moustafa

Received: 31 May 2010 / Accepted: 30 January 2011 / Published online: 15 February 2011
© Springer-Verlag 2011

Abstract Inhaled short-lived radon progenies may deposit in bronchial airways and interact with the epithelium by the emission of alpha particles. Simulation of the related radiobiological effects requires the knowledge of space and time distributions of alpha particle hits and biological endpoints. Present modelling efforts include simulation of radioaerosol deposition patterns in a central bronchial airway bifurcation, modelling of human bronchial epithelium, generation of alpha particle tracks, and computation of spatio-temporal distributions of cell nucleus hits, cell killing and cell transformation events. Simulation results indicate that the preferential radionuclide deposition at carinal ridges plays an important role in the space and time evolution of the biological events. While multiple hits are generally rare for low cumulative exposures, their probability may be quite high at the carinal ridges of the airway bifurcations. Likewise, cell killing and transformation events also occur with higher probability in this area. In the case of uniform surface activities, successive hits as well as cell killing and transformation events within a restricted area (say 0.5 mm^2) are well separated in time. However, in the case of realistic inhomogeneous deposition, they occur more frequently within the mean cycle time of cells located at the carinal ridge even at low cumulative doses. The site-specificity of radionuclide deposition impacts not only on direct, but also on non-targeted radiobiological effects due to intercellular communication. Incorporation of present results into mechanistic models of carcinogenesis may provide useful information concerning the dose–effect relationship in the low-dose range.

Á. Farkas (✉) · I. Balásházy · I. Szőke · B. G. Madas
Health and Environmental Physics Department, Hungarian Academy of Sciences KFKI Atomic Energy Research Institute, Konkoly Thege M. út 29-33, 1121 Budapest, Hungary
e-mail: farkasa@aeki.kfki.hu

W. Hofmann
Division of Physics and Biophysics, Department of Materials Research and Physics, University of Salzburg, Hellbrunner Str. 34, 5020 Salzburg, Austria

M. Moustafa
Physics Department, Faculty of Science, Minia University, Minia, Egypt

Introduction

Upon inhalation, ^{222}Rn and ^{220}Rn progenies can be deposited in the airways of the human lung, where they interact with the epithelial tissue by emitting α, β and γ radiations. Some of the radon and thoron decay products (^{218}Po, ^{214}Po and ^{216}Po, ^{212}Bi, ^{212}Po, respectively) are short-lived alpha emitters, which can transmit large amounts of localized energies to the surrounding cells, thereby causing cellular damages. Since these interactions take place at a microscopic scale, macroscopic doses, although useful in several cases (e.g. whole body irradiation), fail to give sufficient insight into the processes triggered by ionizing radiation. Due to the localized character of alpha particle energy deposition, the whole lung is not an adequate target when assessing cellular biological effects of alpha emitters. However, choosing the most relevant target size for physical, chemical and biological endpoints remains a crucial issue. Earlier experiments addressing the track structure of alpha particles in tissue (Chatterjee and Schaefer 1976; Wingate and Baum 1976) revealed that the ionization–excitation events triggered by a slowing-down alpha particle take place within a cylinder with the alpha particle trajectory as the axis and a radius

depending on its initial kinetic energy. For the energy ranges of alpha particles emitted by the short-lived radon and thoron progenies, this radius varies between 50 and 100 nm, while the length of alpha tracks ranges between 40 and 70 μm. Some constituents of biological matter have sizes compatible with these size ranges (DNA: 2–25 nm, chromosomes: ~1 μm, cell nuclei: ~8 μm, cells: ~10 μm). However, there is increasing evidence that several effects may also occur in the non-hit cells surrounding a hit cell (bystander effects). Therefore, models based on nano- and microscale dosimetry and incorporating, among other mechanisms, intercellular effects have the potential of elucidating biological effects of ionizing radiation in tissue.

To study the interaction between ionizing radiation and bronchial tissue, a number of microdosimetric models have been developed in the past. Such models are, for example, the Track Structure Model (Katz and Hofmann 1982; Hofmann and Heistracher 1996), the Threshold Specific Energy Model (Sedlák 1996) and the so-called LET model of Miller et al. (1996) derived from cellular irradiation experiments. A comparison of these three models can be found in Böhm et al. (2003). Microdosimetric parameters have also been computed by different approaches based on analytical and Monte Carlo techniques (Caswell and Coyne 1990; Hofmann et al. 2000; Nikezic et al. 2002; Fakir et al. 2006, among others). However, most of current models of radon progeny lung dosimetry apply strong simplifications regarding airway geometry, radionuclide deposition and epithelial cell structure. These models assume uniform activities along the airways, which are represented by smooth straight cylinders (for instance, the ICRP model: ICRP66 ICRP Publication 1994; NRC model: NRC, National Research Council (NRC) 1991 or the model of Nikezic and Yu 2001). In reality, however, the bronchial tree is built up of sequentially bifurcating airways, and the deposition distribution of the inhaled radionuclides within the bronchial airways proved to be highly non-uniform (Balásházy et al. 2003; Farkas et al. 2007). Furthermore, radiosensitive cells exhibit complex depth distributions rather than uniform ones (Mercer et al. 1991), as commonly assumed in current models (e.g. ICRP Human Respiratory Tract Model, ICRP66, ICRP Publication 1994). In addition, besides the basal and secretory cells, considered to be the progenitor cells of bronchial carcinomas (Johnson 1995) and used by current models, differentiated cell types (ciliated, pre-ciliated) can indirectly contribute to the promotion of lung carcinomas. For example, differentiated cells may be inactivated by ionizing radiation and force damaged unstable proliferative cells to divide (Truta-Popa et al. 2008).

In recent years, the continuously enhancing computing power and the emergence of complex computational fluid and particle dynamics (CFPD) techniques allowed the computation of inhaled particle deposition patterns in more realistic geometries (Farkas and Balásházy 2008). Since these models can determine the exact location of every emitting radionuclide deposited in the lung, numerical methods based on the simulated deposition patterns are able to compute the exact distances between hit cells or cell nuclei, and, following the incorporation of biophysical processes, the spatial distributions of inactivated and transformed cells, as well. Although a comprehensive experimental study on the effect of spatial distribution of hit cells on different biological endpoints is still missing, it is clear from the existing experimental results that the spatial distribution of activity and related alpha hit distributions are essential for the induced biological damage. Different biological endpoints may be sensitive to the hit pattern. For example, several biological experiments demonstrated that the cell survival probability decreases abruptly with the number of hits a cell receives (Thomassen et al. 1990; Ford and Terzaghi-Howe 1993; Simmons et al. 1996; Kugel et al. 2002). It is evident that the probability of multiple hits will be higher considering realistic inhomogeneous surface activities instead of uniform ones. Based on clonogenic survival data of Mitchell et al. (2002), when all the cells were traversed by exactly one alpha particle, the survival fraction was higher than when only 10% of the cells were irradiated each receiving 10 hits. Oncogenic transformation frequency was also reported to be higher when only a small part of cells received hits than when the same total number of hits was equally distributed among all the cells (Sawant et al. 2001a). It could be demonstrated that even the same hit number distribution (frequency plotted as a function of the number of hits) can produce different effects upon the spatial distribution of the hit cells. If the hit cells are close to each other and form a cluster, the outcome is most probably different from the case when the same hit cells are uniformly distributed, and thus the hit number distribution is the same. Therefore, calculations of the exact spatial patterns of hit, inactivated and transformed cells, involving the knowledge of distances between them, instead of providing only their number distribution or simply assuming that they are uniformly distributed, may be an important step towards a qualitatively better risk assessment.

In addition to the spatial correlations, time distributions of hits, cell deaths, transformations and other events leading to malignancy as a function of the exposure level may promote a better understanding of the mechanisms and effects induced by densely ionizing radiations. Although usually neglected, time after or between two hits may play a major role in radiation biology and risk assessment. One of the simplest examples demonstrating the significance of time as a relevant parameter is the dose rate. It certainly

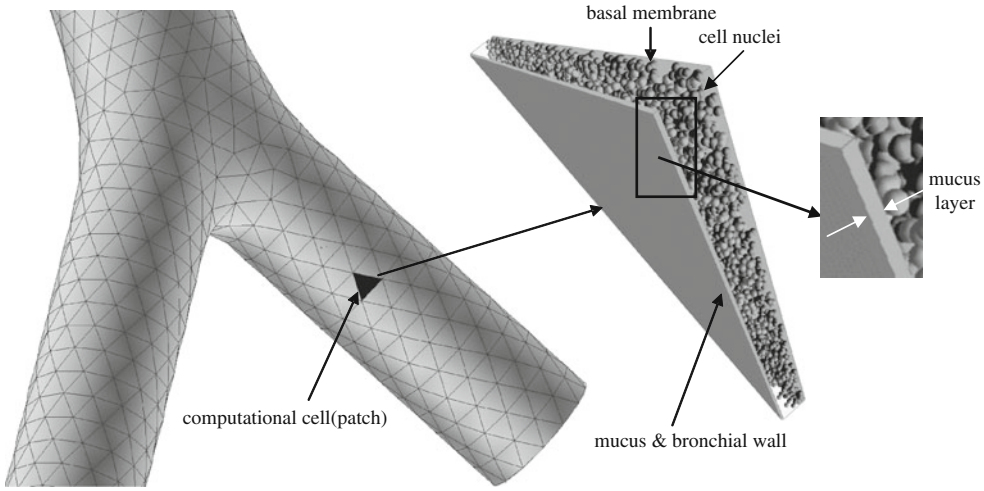

Fig. 1 Mathematical mesh on the surface of a single central airway bifurcation (*left*), and mucus (5 μm) and epithelial cell nuclei (in a 58-μm layer) below the surface of a selected computational cell (*middle*). A piece of the middle image is enlarged to visualize the mucus layer (*right*)

will make a difference for a cell, tissue or organism whether it receives a given amount of energy during a short or a prolonged exposure period. In fact, inverse dose rate effects were reported by a large number of investigators for different biological endpoints and types of radiation (BEIR VII Report 2006). Possible characteristic points of the time scale could be the different repair half times, the cell cycle time or any other time period related to relevant biological processes. Knowledge of the distribution of critical events within the characteristic time periods would enable us to get more insight into the dynamics of the events following radiation exposure and ultimately into the dynamics of carcinogenesis.

Knowledge of spatial and temporal correlations is especially relevant for low doses, where neither epidemiology nor experiments could establish a statistically convincing plausible dose–effect relationship. Thus, the primary objectives of the present study were (1) to quantify inhomogeneous radionuclide deposition and (2) to determine spatial and temporal correlations of different microdosimetric quantities and related biological endpoints associated with low radon exposure levels. This will be achieved by applying morphologically more realistic airway geometry, a more accurate histological structure of the bronchial airway epithelium, and state-of-the-art computational methods.

Methods

This study focuses on the bronchial region of the human respiratory system, because there is clinical evidence that radon-induced carcinomas occur predominantly in the large bronchi. Based on detailed histopathological studies (Veeze 1968; Saccomanno et al. 1996; Kotin and Falk 1959; Churg and Vedal 1996), radon-induced carcinomas arise preferentially in the upper lobes, especially in the right upper lobe. Therefore, a representative central airway segment consisting of a single bronchial bifurcation was considered in the present study (see Fig. 1). The parent tube of the bifurcation is a fourth generation branch, the daughter ones are fifth generation branches from the right upper lobe of the lung (note: the trachea is denoted as generation 1). The above-mentioned three-dimensional bifurcation is characterized by the morphometric data summarized in Table 1 and was constructed by the numerical technique described by Hegedűs et al. (2004).

Table 1 Geometric data of from fourth to fifth generation bronchial airway bifurcation model

Length of parent branch (cm)	0.76
Length of daughter branches (cm)	1.27
Diameter of parent branch (cm)	0.56
Diameter of daughter branches (cm)	0.45
Bifurcation angle (°)	70.00
Curvatures radii (cm)	1.42
Curvature radius of carinal rounding (cm)	0.50

To get the expected locations of the depositing radioactive particles, it is necessary to track them within the airways. Since particle trajectories are strongly influenced by airstreams, only a coupled (particle–air) approach can yield appropriate results. In the present study, a one-way coupling was assumed, which means that the fate of the particles depends on the velocity of the moving air, but the airflow is not influenced by the inhaled particles due to the low particle concentrations considered. Air- and particle transport within the model airway bifurcation was simulated by the FLUENT CFD (computational fluid dynamics) code (FLUENT User's Guide 2001) after discretizing the computational domain. By the application of a numerical mesh, the whole geometry was divided into discrete volume elements. Air velocities and pressure values in the computational cells were computed by solving the mass

Table 2 Breathing and aerosol parameters characteristic of uranium mines used in the present study

Breathing parameters	Breathing mode	Nose breathing (ICRP 66, 1994)
	FRC (l)	3.3 (ICRP 66, 1994)
	Tidal volume (l)	1.25 (ICRP 66, 1994)
	Breathing cycle (s)	3 (ICRP 66, 1994)
Aerosol parameters	AMAD (nm)	Attached: 200 (BEIR VI, 1999)
		Unattached: 1 (BEIR VI, 1999)
	Unattached fraction (%)	1 (BEIR VI, 1999)
	Activity concentration ratios ($^{218}Po/^{214}Pb/^{214}Bi$)	0.6/0.29/0.21 (BEIR VI, 1999)
	Equilibrium factor	0.3 (BEIR VI, *1999*)
	PAEC (WL)	0.52 (Tomasek et al. 2008)

FRC functional residual capacity, *AMAD* activity median aerodynamic diameter, *PAEC* potential alpha energy concentration

and momentum conservation equations. Details of the air velocity computing numerical schemes and particle tracking algorithms were presented in our earlier works (Farkas et al. 2006; Farkas and Balásházy 2007, 2008).

In the present study, breathing and exposure conditions characteristic of uranium mines were assumed. The decision on using exposure data of uranium mine environments is justified by the availability of large datasets of mines from all over the world including mines with relatively low, moderate and even very high exposure levels (BEIR VI Report 1999). The exposure data used in the present study are summarized in Table 2.

Breathing parameters (functional residual capacity, tidal volume and breathing cycle), which were selected from ICRP66 (1994), correspond to light physical activity of an adult male. Breathing data from Table 2 are in good agreement with breathing rates derived by Ruzer et al. (1995) for underground metal miners in Tadjikistan and are also consistent with those published in ICRP66 (ICRP Publication 1994) for heavy workers in South African gold mines. Because of the relatively low concentrations of thoron decay products, only the short-lived alpha emitter daughters of ^{222}Rn were considered. Aerosol parameters in Table 2 are primarily based on BEIRVI Report (1999), consistent with the recently published values of Marsh et al. (2008). Furthermore, the average exposure level characteristic of the well-documented Czech uranium mines (Tomasek et al. 2008) was adopted in our calculations.

Discrete particles were injected into the computed flow field of the model bifurcation (airway generations 4–5) taking into account the aerosol deposition in the upper airways and in the bronchi preceding the model bifurcation (generations 1, 2 and 3). The number of radionuclides deposited in the extrathoracic airways and in the bronchi leading to the model bifurcation was computed by the most recent version of the stochastic lung deposition model, initially developed by Koblinger and Hofmann. A detailed description of the stochastic lung model and its further developments can be found in Koblinger and Hofmann (1985, 1990), Hofmann and Koblinger (1990), Hofmann et al. (2002 and 2006). The number of inhaled particles depends on the radioaerosol concentration of mine environment, breathing conditions and time of exposure.

For the quantification of particle deposition, deposition efficiencies (η) and deposition enhancement factors (DEF) were computed. By definition, the deposition efficiency is the ratio of the number of particles deposited in a given airway segment to the number of particles entering that same segment. Furthermore, the deposition enhancement factor is defined as the ratio of local to average particle deposition densities. Deposition densities are computed as the number of the particles deposited on a given surface divided by the surface area. For this purpose, the whole surface of the airway bifurcation was scanned by a prespecified surface element following the technique originally described by Balásházy et al. (1999). Since both the maximum value of DEF and its distribution are functions of the scanning patch size, selecting a mathematically and biologically plausible patch size is a delicate task. In the present study, the patches are triangle-shaped with the edges of the triangle equal to 1 mm. This size coincides with the current estimate for the range of the bystander effect around an irradiated cell (Belyakov et al. 2005; Shuryak et al. 2007). Recently, Leonard (2009) and Gaillard et al. (2009) published bystander range values that are somewhat lower: 0.21 and 0.1 mm, respectively. At the same time, it should be recognized that this range certainly depends on the type of cells, biological endpoint, type of radiation, mechanism of cellular interaction and other factors. Regarding the dependence of bystander range on the type of signalling mechanism, it should be noted that some of the existing models either do not incorporate any signalling mechanism (Brenner et al. 2001; Little and Wakeford 2002; Jovanovic and Nikezic 2010) or deduce universal equations of bystander signal propagation (Shuryak et al. 2007; Fakir et al. 2009) regardless to the mediating pathway (through gap junction channels or by soluble factors). In a series of bystander models, it is assumed that the intercellular communication is due to the

diffusion of secreted molecules emitted by hit cells and eventually intercepted by non-hit bystander cells (Ballarini et al. 2006; Nikjoo and Khvostunov 2003). Published mathematical models operate with distances ranging from 0.1 mm to a few millimetres (see Shuryak et al. 2007; Ballarini et al. 2006; Fakir et al. 2009), in accordance with the values reported by Belyakov et al. (2005), Leonard (2009) and Gaillard et al. (2009). Hence, as a first modelling approximation, our triangular-shaped computational cell with a 1-mm edge size seems to be a reasonable assumption.

In order to model the interaction of the radiation with radiosensitive epithelial cell nuclei, alpha tracks were generated, and a three-dimensional bronchial epithelium was constructed (see also Szőke et al. 2008). Alpha tracks were simulated as straight lines with randomly selected directions. Their lengths (ranges) were derived from the initial kinetic energies of alpha particles and published stopping power functions for air and tissue (ICRU 1993). Near-wall and far-wall alpha tracks were distinguished by their direction. By definition, tracks entering directly the tissue are near-wall alpha tracks, whereas tracks first entering the airway lumen and then penetrating into the epithelium are far-wall alpha tracks. The reconstruction of the three-dimensional bronchial cell nucleus structures is based on the histological data of Mercer et al. (1991). In this work basal, indeterminate, ciliated, pre-ciliated, goblet and other secretory cell nuclei types were considered. Using cell nuclei instead of cells raises again the question of the appropriate targets. Increasing experimental evidence has shown that the traversal of a cell nucleus by tracks is not a prerequisite for triggering a direct (Wu et al. 1999) or bystander (Shao et al. 2004) response. Nevertheless, by using cell nuclei, the present results become comparable to those published in the literature, since most of the earlier models dealt with nuclei. Our model is structured in a way so that switching from nuclei to cells is merely a technical question. Since the probability of hit is proportional to the square of target diameter, by using cells instead of cell nuclei the hit probabilities of the targets will generally increase. Similarly, the amount of the deposited energy will also increase (but in a quasi linear manner), because of the increase in chord (the length of an alpha particle's pathway inside the target) lengths. Since mass increases with the cube of diameter, the expected values of cellular doses (Madas et al. 2010) are similar to the expected values of cell nucleus doses (Szőke et al. 2008).

Based on the intersection of near-wall and far-wall alpha tracks with the generated cell nuclei, alpha hit probabilities, chord length and LET (linear energy transfer) values can be computed. Chord length and mean LET (energy deposited in the cell nucleus along a chord divided by the chord length) values were used as input parameters for the determination of biological endpoints. Cell inactivation and cell transformation probabilities were computed by the application of the Unit-Track-Length model of Crawford-Brown and Hofmann (1991). Hit probabilities and inactivation probabilities were computed for each type of cells mentioned above, including both proliferative and terminally differentiated cells. However, transformation probabilities were computed only for the radiosensitive basal and goblet (secretory) cells.

To quantify the spatial distribution of the computed microdosimetric parameters and the biological endpoints, two different methodologies were developed. The first procedure is based on the computation of the distances of each hit cell nucleus to its nearest hit neighbour. The second method consists of scanning the whole bifurcation with the pre-specified surface element (patch) and counting the cells which received alpha hits. This method works in a manner similar to the algorithm developed for the computation of DEF values (see above), but it stops after computing the hit (inactivation, transformation) densities (i.e. it does not divide the local densities by the average density). It is worth noting that the thickness of the patch was constantly 63 μm, consisting of a 58-μm-thick epithelium and a 5-μm-thick mucus (see Fig. 1).

Time distributions of alpha hits and biological endpoints were simulated by assuming that for a given exposure level the surface activity distribution of the deposited radon daughters is constant in time. This implies that equilibrium has been reached between airway deposition and radioactive decay. This assumption might not describe correctly the case of fractionated exposures, but it is still a fairly reasonable approximation for chronic exposures.

It is worth mentioning that particle clearance, which is not taken into account in this approach, may modify to some extent the time and space distributions of the deposited activity. Although there are several clearance mechanisms at play in the bronchial region, the mucociliary clearance is the major determinant for deposited short-lived progenies. Implementation of algorithms to simulate how mucus removes the deposited particles from the investigated airway segment towards the pharynx and transports others from the deeper regions of the lung up to the targeted bifurcation is currently in progress.

In the present work, space and time distributions of the selected microdosimetric parameters and biological endpoints were computed for both uniform and inhomogeneous particle deposition distributions, in order to reveal the differences between the two scenarios in terms of the resulting biological effects, and to highlight the role of considering realistic radionuclide deposition.

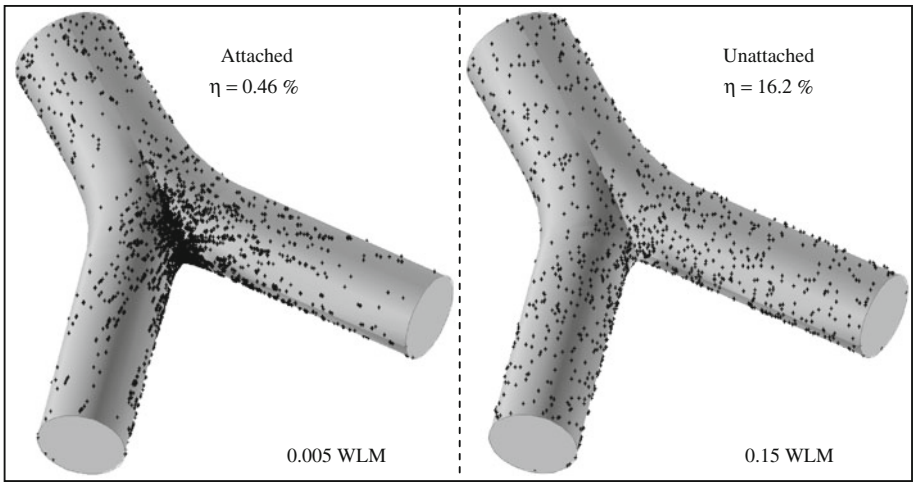

Fig. 2 Deposition patterns of inhaled attached (*left panel*) and unattached (*right panel*) radon progenies at two different exposure levels. η denotes the deposition efficiency

Results and discussion

Simulations performed with the stochastic lung model for the breathing data presented in Table 2 demonstrated that 3.3% of the inhaled attached and 82% of the unattached radon progenies are trapped in the nasopharyngeal upper airways. Likewise, 0.06% of the inhaled attached and 2.47% of the unattached radon decay products deposit in the tracheobronchial airways (generations 1–3) upstream of the targeted bifurcation in Fig. 1 (generations 4–5). Taking into account these deposition results and exposure data in Table 2, the number of attached progenies entering the model bifurcation is 8.8×10^7/WLM, while the number of unattached progenies is 1.5×10^5/WLM. Deposition patterns of attached and unattached progenies in the modelled bifurcation unit are presented in Fig. 2.

Because of the small percentage of the unattached progenies in the modelled environment and the high nanoparticle filtering efficiency of the upper airways, many more attached particles reach the large bronchial bifurcations, like the one shown in Fig. 1, than unattached particles. In order to visualize the differences between the deposition patterns of attached and unattached radon daughters, roughly the same number of deposited particles is presented in Fig. 2, which implies that the WLM values in the two panels of Fig. 2 are different. This figure demonstrates that in this section of the airway system, the deposition efficiency of the unattached fraction is much higher than that of the attached fraction. Furthermore, the deposition of the attached fraction is more site-specific, with deposited particle accumulations at the peak of the bifurcation. The deposition density of the attached and unattached particles can be quantified in terms of deposition enhancement factors, as described in the "Methods" section. Large-scale computations revealed that deposition density values of the radon decay products (attached + unattached) on some of the surface elements can be more than one order of magnitude higher than the average deposition density (Fig. 3), indicating that the activity is distributed highly inhomogeneously along the surface of bronchial airways.

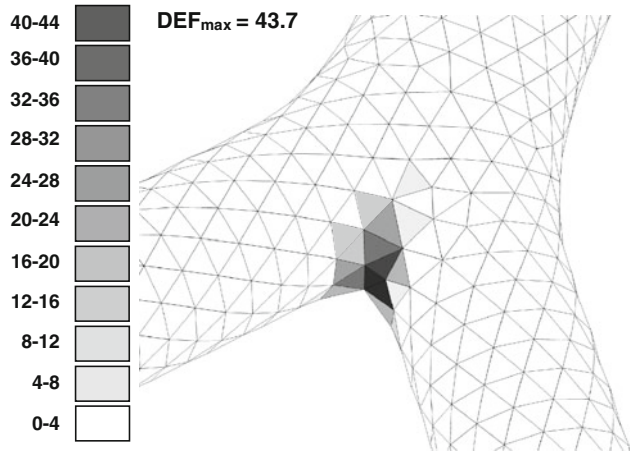

Fig. 3 Gray levels of computational cells corresponding to computed deposition enhancement factor values. Patch size: 0.43 mm^2, DEF_{max}—maximum deposition enhancement factor

The inhomogeneous radon progeny deposition suggests that the radiation burden of epithelial cells is also non-uniform along the airways. Hence, the assumptions of uniform activity distributions and average cellular/cell nucleus doses instead of realistic distributions might not be fully appropriate. However, before exploring the effect of the inhomogeneously distributed activity on cellular alpha hits, single hit probabilities assuming uniform activity distribution were computed and compared with corresponding data available in the published literature (see Table 3) to validate the hit model.

James et al. (2004) presented results obtained by applying both the ICRP66 (ICRP66 1994) and Ro90 (Robbins et al. 1990) epithelium models. Since in most of the earlier publications, the probability that an epithelial

Table 3 Comparison of the present results on the hit probability per bronchial cell nucleus corresponding to uniform activity with data published by different investigators

Source	Hit probab./WLM, basal	Hit probab./WLM, secretory
Nikezic and Yu (2001)	0.011	0.039
Hui et al. (1990)	0.015	0.021
James et al. (2004), ICRP66 model	0.008	0.032
James et al. (2004), Ro90 model	0.021	0.046
Present model, uniform activity	0.024	0.041

cell nucleus is hit is provided for basal and secretory cells, for this comparison the probabilities were computed separately for the two types of cells. As the table demonstrates, there is no significant difference in terms of single hits per bronchial cell nucleus between the present results and the data available in the published literature. The differences may be due to the different approaches regarding particle deposition and the cellular structure of the epithelium. However, all the investigators listed in Table 3 dealt with uniform surface activities, which according to Fig. 2 is a somewhat arbitrary assumption. Although the site-specific deposition causes non-uniformity at the level of cell nucleus hits, the degree of inhomogeneity is certainly lower than that of the primary deposition because of the far-wall alpha tracks. Approximately half of the alpha particles do not enter the tissue directly, but first enter the lumen and then penetrate into the epithelium at different locations hitting the bronchial cells/cell nuclei. To determine the exact spatial distributions of the hit cell nuclei, the distance of every hit cell nuclei to its nearest hit neighbour was calculated assuming both uniform and inhomogeneous particle deposition scenarios. Figure 4 demonstrates the distribution of these distances, characterizing to some extent the cluster formation of the hit cells. Note that the distribution of different powers of the distance between hit nucleus first neighbours could also be computed, but since it is not known which power is more relevant from a radiobiological aspect, the simplest, i.e. the linear approximation has been applied.

It is somewhat puzzling at first glance that although there is a significant difference between uniform deposition and inhomogeneous deposition patterns, the distribution of the above distances is very similar in the two cases. However, a detailed analysis of the apparent similarity of the distributions revealed that nuclei hit by the same alpha particle make an important contribution to the peak of the distribution shown in the upper panels of Fig. 4. The middle panels of the same figure show an example, when uniform and accumulated particle deposition yield the same distance distribution. Note that the middle panels of Fig. 4 have a rather illustrative role and thus the scales are not fully realistic. A more informative parameter for the characterization of the non-uniform burden could be the number of hit nuclei per patch (predefined surface element). Inspection of the bottom panels of Fig. 4 demonstrates that the distribution of this parameter is clearly different in the two cases. In case of uniform particle deposition, the number of hit cell nuclei per patch is distributed around a mean value. Assuming realistic deposition patterns, the majority of the patches contain only a small number of hit cell nuclei, or even no hits, while some surface elements may contain 20 times the average number of hit nuclei. For a better comparison of the two distributions, the fine structure of the hit distribution corresponding to realistic particle deposition is shown for the interval 0–250 hits/surface element in the insert of the right bottom panel. In this approximation, each patch is represented by a specific average hit probability value, which can be computed based on the number of hits/patch and the number of cell nuclei belonging to a patch. Figure 5 depicts the dependence of the number of hit nuclei per patch as a function of WLM for the most exposed patch. For comparison, the same dependence is plotted for the mean number of hit nuclei per patch. As the figure reveals, the inhomogeneity in the distribution of hit cell nuclei per patch is present at any exposure level in the low-dose range. This result suggests that although the proportion of cell nuclei receiving hits is quite low in the low-dose range, there are areas, where the number of hit nuclei is very high and thus the most exposed cells are close to each other. The above fact is usually neglected by current risk models, which deal with average hit numbers.

It is important to note here that computations related to Figs. 4 and 5 do not account for multiple hits. Thus, considering multiple hits, the inhomogeneity becomes even more accentuated. The locations of the cell nuclei receiving multiple hits are illustrated in Fig. 6.

Assuming realistic particle deposition patterns, the probability that a cell nucleus located in the carinal ridge of the airway bifurcation receives multiple hits is much higher than for a nucleus from the cylindrical parts of the bifurcation. Comparing the multiple-hit patterns in the right panel of Fig. 6 to the deposition patterns in Fig. 2, it can be seen that besides the peak of the airway bifurcation, which is the preferential deposition site, the central part, that is the bifurcation zone situated between the cylindrical parts of the parent and daughter airways, also receives multiple hits. The difference between the deposition and multiple-hit

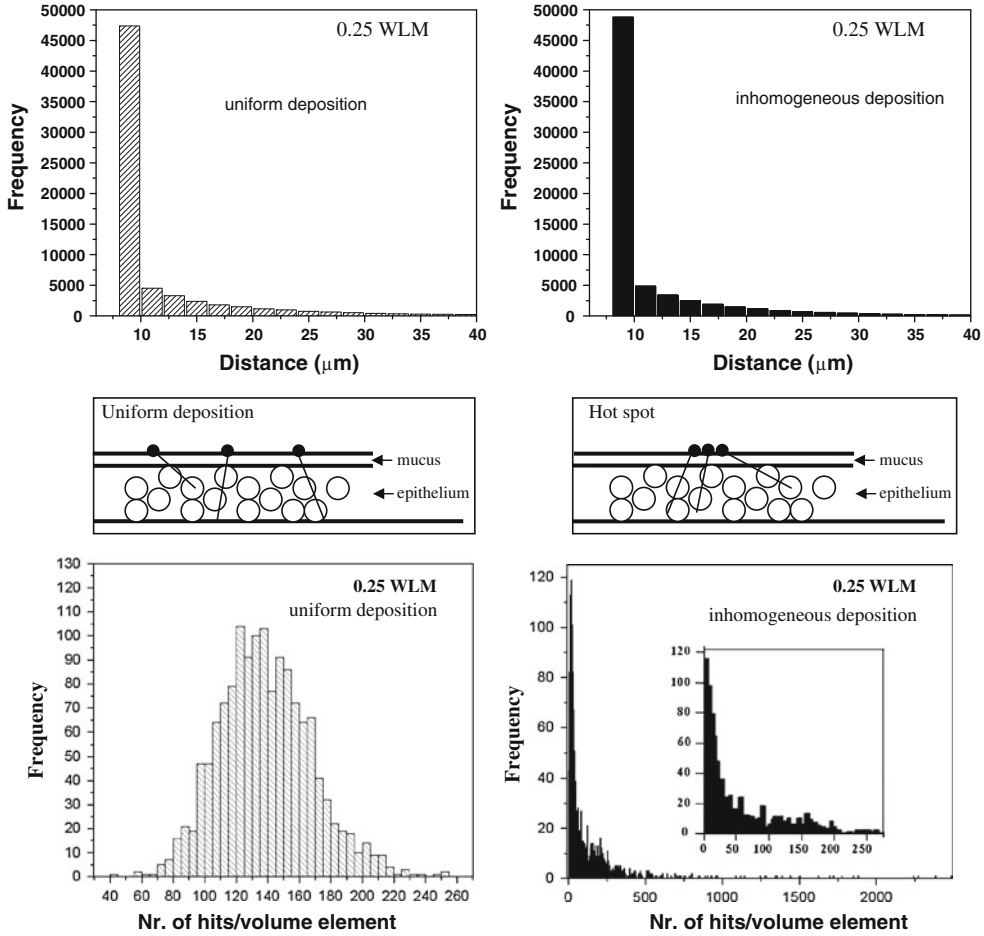

Fig. 4 *Upper panels* Distribution of the nearest distances of hit cell nuclei assuming uniform (*left*) and inhomogeneous (*right*) deposition of radionuclides on the bronchial airways. *Middle panels* Two specific cases, when uniform and inhomogeneous depositions result in similar nearest distance distributions. *Bottom panels* Distribution of the number of hit cell nuclei located in a pre-specified surface element assuming uniform (*left*) and inhomogeneous (*right*) particle deposition distributions

patterns is mostly due to the far-wall alpha tracks starting from the vicinity of the peak of the bifurcation and traversing first the airway lumen and then penetrating into the tissue. Assuming inhomogeneous particle deposition, the mean value of the distances of cell nuclei receiving multiple hits to their multiple-hit neighbours (d_m) is also significantly lower than the same parameter for uniform deposition, indicating that cells at direct risk are closer to each other when assuming realistic deposition scenarios. As demonstrated in Fig. 7, the increase in WLM leads to the decrease in d_m, suggesting that multiple-hit nuclei are located closer to each other at higher exposures. The curve in Fig. 7 saturates at high doses because d_m certainly cannot be smaller than the distance between two neighbouring cell nuclei.

The number of multiple-hit cell nuclei in the hot spot as a function of WLM is plotted in the upper panel of Fig. 8. For comparison, the average number of nuclei receiving multiple hits per patch is also shown. As the figure

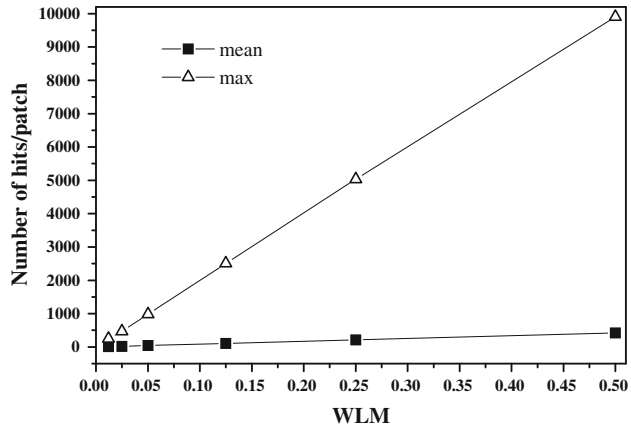

Fig. 5 Average and maximum number of hits per surface element as a function of WLM

demonstrates, the density of multiple-hit nuclei can be more than twenty times higher in the hot spot than its average value. To see whether the observed tendencies

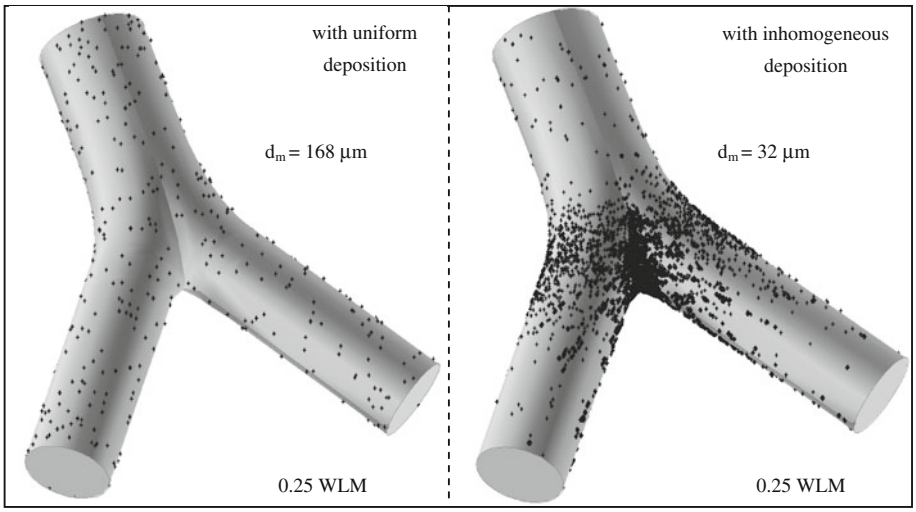

Fig. 6 Locations of cell nuclei receiving multiple hits in case of uniform (*left panel*) and realistic non-uniform (*right panel*) radionuclide surface distributions. d_m denotes the mean value of the distances between the nuclei receiving multiple hits and their nearest neighbours receiving multiple hits

hold for higher exposure levels as well, probabilities that a cell nucleus receives at least two hits, at least three hits, etc. were computed. Assuming uniform radionuclide deposition, the probability of single and double hits in the considered working level range increases linearly with the increase in the exposure level. However, there is little chance (computed probability: 0.043) for a nucleus to receive a double hit below 6 WLM and the probability of more than two hits is practically zero. In contrast, in the hot spot of the inhomogeneous deposition, the curves are non-linear and the probability of two, three and even four hits is very high even at low exposure levels, suggesting that for these regions of the tissue the "low-dose problem" is actually a "high-dose problem".

Regarding the related cell biological consequences, cell inactivations and transformations were computed in a manner described in detail in the "Methods" section. The results of these simulations are presented in Fig. 9.

The figure reveals that following the tendencies of the microdosimetric parameters illustrated in Figs. 2, 3, 4, 5, 6, 7 and 8, the spatial distribution of the biological endpoints is also heterogeneous. While the average number of inactivated cells in a patch is 33.5 at 0.125 WLM, it reaches 766 in the hot spot. The corresponding values for 0.5 WLM are 123.8 and 1,185, respectively.

It has been demonstrated in different experimental studies that the transformation frequency due to ionizing radiation is extremely low in the low-dose range (Miller et al. 1999; Sawant et al. 2001a). For instance, according to Miller's microbeam irradiation experiments performed on CH310T1/2 cells (Miller et al. 1999), only one cell out of ten thousand surviving cells receiving exactly one hit will be transformed. Applying the computational schemes described in the "Methods" section, the average number of transformed cells on a patch is 0.046 at 0.125 WLM and 0.17 at 0.5 WLM. However, our computations

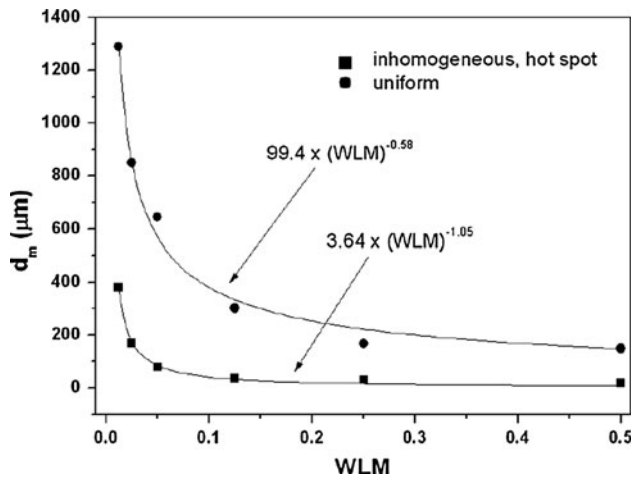

Fig. 7 Mean value of the distances of cell nuclei receiving multiple hits to their nearest neighbour nucleus receiving multiple hits as a function of exposure in WL in the deposition hot spot assuming inhomogeneous particle deposition, and in an arbitrary patch in case of uniform radioisotope deposition

demonstrated that even at low exposures and hence low average transformation probabilities, there were three transformed cells at 0.125 WLM and five at 0.5 WLM in the hot spots. It is worth mentioning that one patch corresponds to about 23,300 cells (Mercer et al. 1994). The existence of a significant number of cell death and cell transformation events in restricted areas suggests that extensive detrimental effects might occur even in the low or intermediate dose range. However, to validate the results of model computations, further biological experiments focused on the triggering and detection of such local effects are required.

Besides the aspects highlighted above, knowledge of the exact space correlations may also be important from the non-targeted effects point of view. Several mechanisms affecting the unirradiated neighbours of the irradiated cells

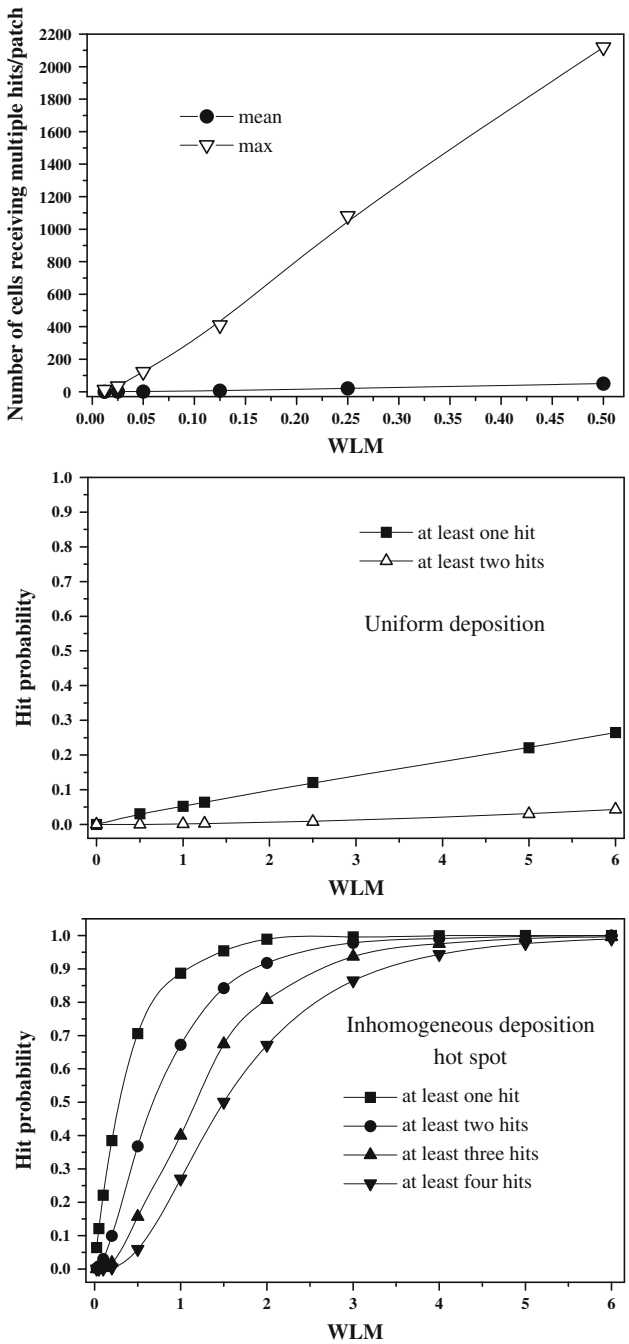

Fig. 8 Average and maximum number of multiple hits per surface element as a function of WLM (*upper panel*). Hit probability assuming uniform deposition distribution (*middle panel*) and in the hot spot of the inhomogeneous deposition (*bottom panel*)

were reported by different investigators (Zhou et al. 2000; Belyakov et al. 2006; Iyer and Lehnert 2000; Lorimore et al. 1998; Bowler et al. 2006, among others). Although the exact underlying mechanisms and spatial patterns of these bystander effects are not yet fully understood, it is evident that knowledge of the spatial distribution of the irradiated (directly hit) targets is essential also in the perspective of nontargeted effects. For example, Schettino et al. (2005) have demonstrated that, at least in vitro, triggering of a bystander signal is a binary process and deduced a relationship between the signal induction probability and the dose that a cell receives. It has been proven by Fakir et al. (2009) that the probability of producing a single signal when two cells are hit each by one alpha particle is different from the probability of having one signal when one of the cells receives two hits, while the other cell is not hit. Furthermore, the probability of the emission of two signals after two hits is also different in the two cases (zero in the case when one of the cells receives both hits).

In the present study, we propose to illustrate the significance of the spatial pattern of the hits in the case of non-targeted effects, as well. Bystander effect, adaptive response and induced apoptosis are non-targeted effects, which are relatively easy to simulate due to the large amount of available quantitative experimental data. Since our bystander model is under publication, we will not simulate this phenomenon here.

Adaptive response is described as the reduced effect of radiation received as challenging dose if induced by a previous low radiation dose, the so-called priming or conditioning dose (Tapio and Jacob 2007). This phenomenon has been observed in vitro and in vivo using various indicators of cellular damage. However, all the available research results indicate that adaptive response is observable if the priming dose is low (say 20 mGy). Average cellular doses due to single alpha particles emitted by radon progenies are more than ten times higher, small doses ($0\ \text{mGy} < D < 20\ \text{mGy}$) occurring quite rare. Therefore, it is not probable that cells receiving such high doses followed by similar doses will exhibit adaptive response. This is also the reason why published studies addressing adaptive response do not use alpha particles to deliver the priming dose. For this purpose, usually X (e.g. Sawant et al. 2001b) or γ rays (Mitchel et al. 2004; Ina et al. 2005, among others) are used. In a limited number of studies, high LET neutrons were also used (e.g. Marples and Skov 1996) to achieve small priming doses. Thus, adaptive response due to consecutive alpha hits was not addressed in this work. However, induced apoptosis, which has been also investigated in our study (Fig. 10), can be regarded as a kind of "nontargeted adaptive response" reducing the risk. On the other hand, some of the radon daughters are beta- and gamma active (^{214}Po, ^{214}Bi) and thus may provide priming doses for the subsequent alpha decay of ^{214}Po. However, radiation types other than alpha have not been considered in the present work.

In the present study, the relevance of exact spatial distributions of damaged cells in non-targeted effects has been demonstrated through induced apoptosis. It is known that

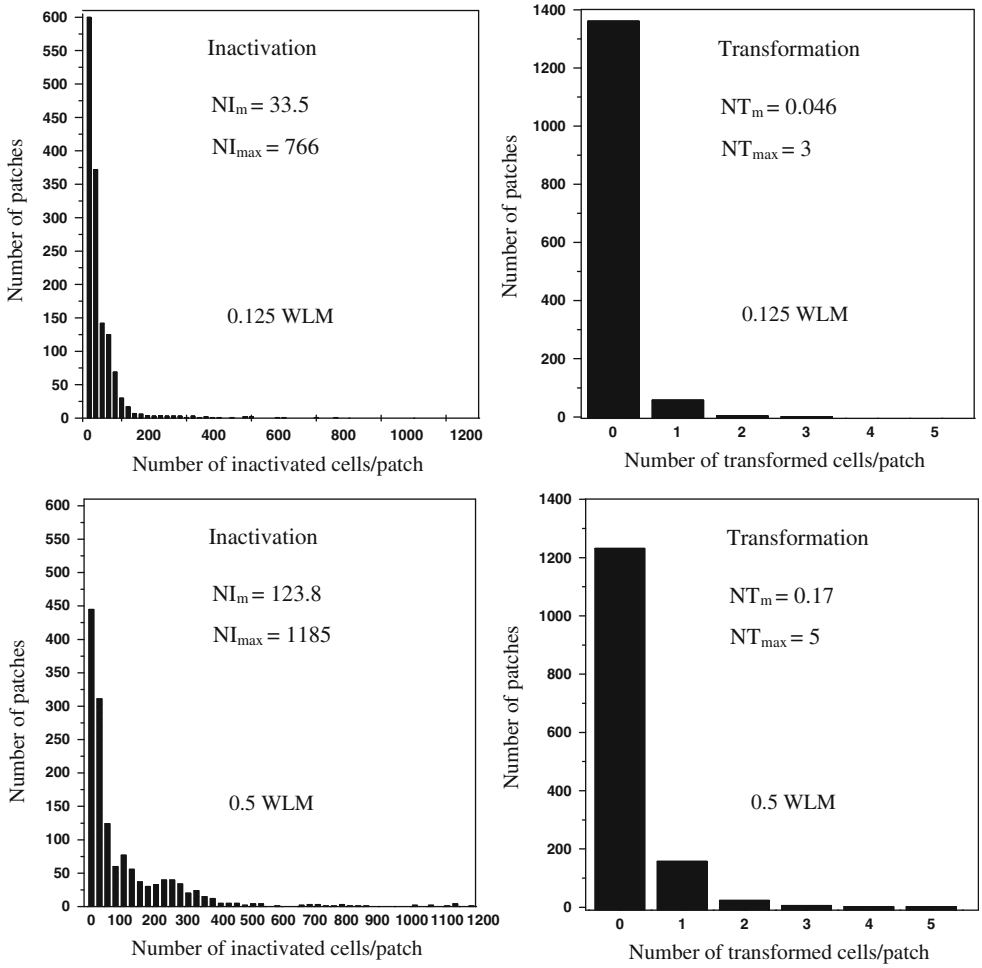

Fig. 9 Distribution of the number of inactivated (*left panels*) and transformed (*right panels*) cells in a given surface element for 0.125 WLM (*upper panels*) and 0.5 WLM (*bottom panels*) exposures, assuming inhomogeneous deposition patterns. NI_m—mean number of inactivated cells/patch; NI_{max}—maximum number of inactivated cells/patch; NT_m—mean number of transformed cells/patch; NT_{max}—maximum number of transformed cells/patch

transformed cells can be eliminated by their non-transformed neighbours. Bauer (2007) described this kind of intercellular-induced apoptosis as a process which, similar to the autocrine self-destructive apoptosis, is mediated by radical oxygen species (ROS). Low doses of ionizing radiation can further promote this potential step against oncogenesis by stimulating non-transformed cells to force the transformed neighbours into apoptosis (induced apoptosis). The dose dependence of induced apoptosis was analysed by Portess et al. (2007). The upper panel of Fig. 10 illustrates the excess of apoptotic cells due to irradiation, that is, the percentage of cells suffering intercellular-induced apoptosis above the control as a function of absorbed dose. For modelling purposes, a non-linear curve was fitted to the measured data points of Portess et al. (2007). To analyse the effect of non-uniform radioaerosol deposition, the percentage of induced apoptosis (above the control, without radiation exposure) was calculated for uniform deposition and for the cells underlying the deposition hot spot. Since the vertical axis is labelled as percentages, there will be no difference between considering the whole geometry or a randomly selected patch in case of uniform deposition. The bottom panel of Fig. 10 demonstrates that higher local doses enhance the induced apoptosis of the transformed cells. By the same token, due to the high local burden characterizing the hot spot, induced apoptosis saturates at a quite low exposure level (between 0.1 and 1 WLM, filled circles). The curves corresponding to the two deposition scenarios approach each other, and there will be no significant difference in bystander mediated apoptosis between the hot spot and any patch of the bifurcation with uniform activity above 10 WLM.

The results presented in Figs. 1, 2, 3, 4, 5, 6, 7, 8, 9 and 10 demonstrate the importance of the spatial distribution of the activity, cell nucleus hits and the events leading to malignancy in the study of health effects of inhaled radionuclides and in risk assessment. For instance, several mathematical models of radon-induced cancer risk use the alpha-hit probability at a given radiation burden as an input parameter. Harley and Chittaporn (1996) and Heidenreich et al. (2001) used constant hit probabilities/WLM for basal and secretory cells. Truta-Popa et al. (2008) selected the actual number of hits from a Poisson distribution with known average number of hits. As a result of the present

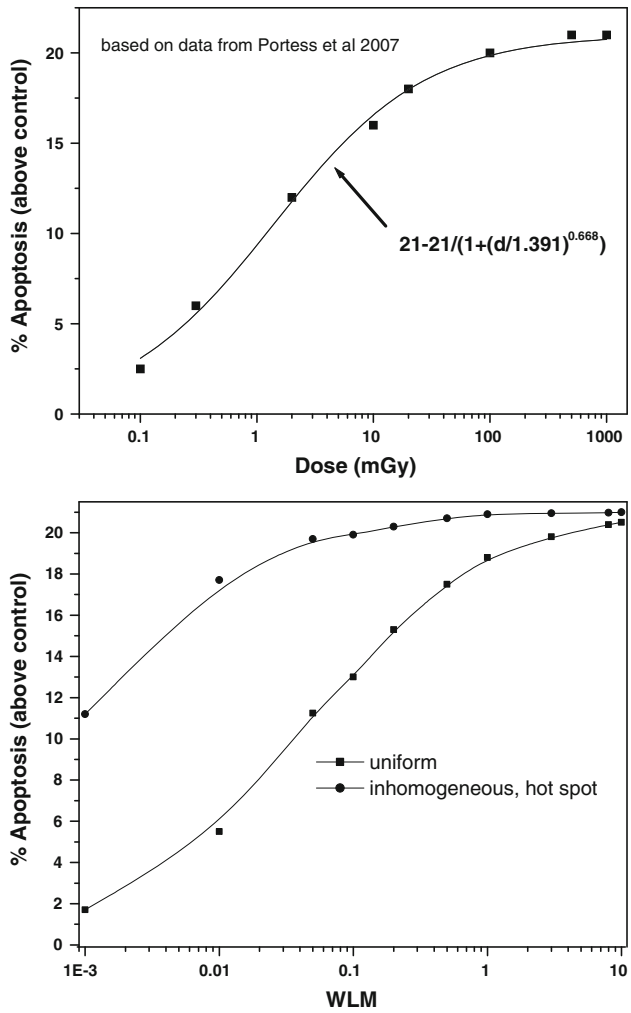

Fig. 10 Percentage of apoptotic cells above control based on data of Portess et al. (2007) (*upper panel*) and corresponding results obtained by present model computations (*bottom panel*) throughout the whole tissue assuming uniform activity distribution and in the hot spot of the inhomogeneous activity distribution. *d* denotes the absorbed dose

computations, the exact number of hits (or hit probability/WLM) for each cell is available and can be applied by future risk models.

However, the production of biological damages, eventually leading to carcinogenesis, is a dynamic rather than a static process. Therefore, accurate models of these processes should incorporate time as an important parameter. In the present study, the probability of multiple hits within a given time interval for different working levels (activity concentrations) was calculated. From a biological damage point of view, the time between two successive hits plays a significant role. One critical value of the time interval between successive hits is certainly the cell cycle time. However, in the case when the time interval is longer than the cell cycle time, not the initial cell, but one of its descendants will be hit (in case of replicative cells) and the related biological effect may be different.

The upper panel of Fig. 11 presents the probability of multiple nuclear hits within an average cell cycle time of about 30 days (Adamson 1985) as a function of exposure level (WL). The two curves correspond to a uniform surface activity distribution and to the hot spot of a realistic activity distribution. The mean working levels of a couple of uranium mines are also marked in the figure. It can be seen that assuming uniform particle deposition, the probability that a cell nucleus receives multiple hits during a cell cycle is extremely low for each of the mentioned mines. The multiple-hit probability values computed for a typical epithelial cell cycle time (30 days), assuming uniform activity along the airways, are consistent with those reported by James et al. (2004) for basal and secretory cells using the ICRP66 reference model (ICRP66 1994). For instance, James et al. (2004) have found that at a 10-WL exposure in a mine the probability of multiple hits is 0.33% for basal and 4.4% for bronchial secretory cell nuclei. At that same exposure, our computations yielded a probability of multiple hits of 0.8%, when averaged over the six types of cells. The difference can be explained by the application of different epithelial morphologies. Likewise, the probability of multiple hits within a cell cycle for the working level characteristic of some of the mines is almost 100% in the hot spot of a realistic particle deposition pattern. There is biological evidence that the fate of a cell depends also on the cycling state (G1, S, G2, M or G0) the cell is traversing when it is irradiated (Miller et al. 1992). The above statement remains valid for multiple hits as well. Thus, parameters like the probability of multiple hits during a sensitive cell cycle phase (e.g. M phase) or the probability of multiple hits within the repair half time may be useful in risk assessment. Most probably, it is a considerable shock for a cell to receive a second hit during repair. In this case, unrepaired damages can interact with those produced by the second traversal (Sutherland 2006). However, the overall damage caused by the two hits within the repair time also depends on the time interval the hits follow each other (Hall and Giaccia 2006). The higher this time interval the smaller the damage will be, because of the repair of sublethal damage caused by the first traversal. It is worth noting that the remaining three R's, namely redistribution, repopulation and reoxygenation, are not expected to play a major role here (Yarbro et al. 2005). The probability of multiple hits in a specific phase can be directly determined from the upper panel of Fig. 11 if the ratio of time a cell spends in a given phase to the cell cycle time is known. For instance, Puck and Steffen (1963) published a mean value of 5.4% for the radiosensitive mitotic phase. In this case, rescaling of the horizontal axis by multiplying the working level values by 18.5 would yield the probability of multiple hits during the M phase as a function of WL. Since ionizing radiation can modify the duration of cell phases and cell

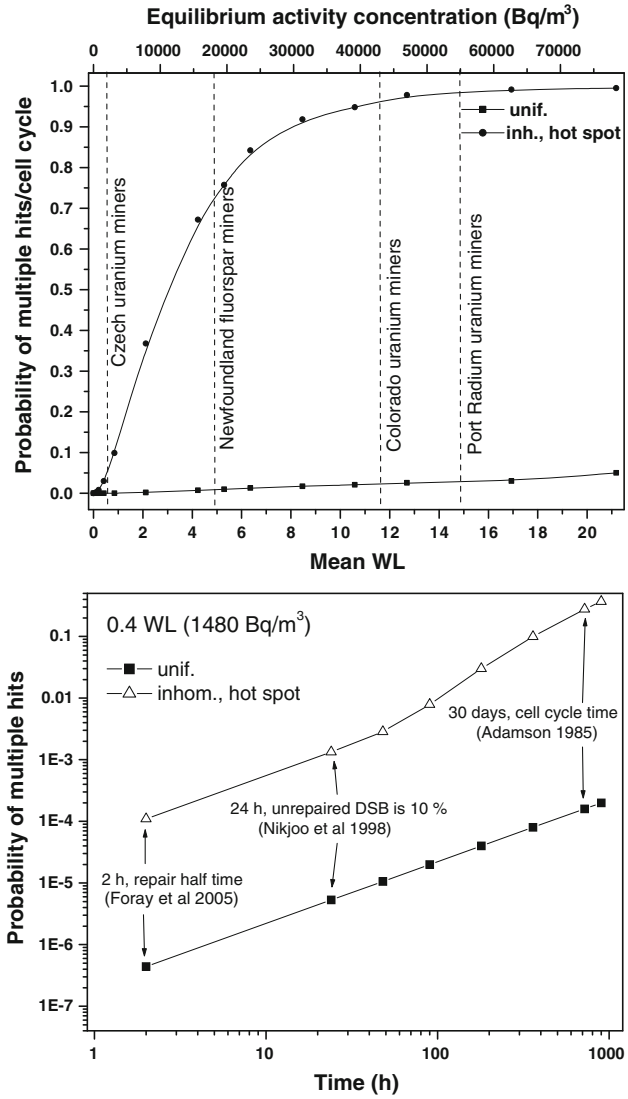

Fig. 11 *Upper panel* Probability of multiple hits during a single cell cycle time (30 days) as a function of the mean exposure level (WL) (*bottom axis*) and equilibrium activity concentration (*top axis*), assuming uniform radon decay product airway deposition, and in the hot spot of the inhomogeneous deposition pattern. *Bottom panel* Probability of multiple hits as a function of time assuming a constant (0.4 WL) exposure level for uniform and inhomogeneous deposition scenarios

cycle times (Fournier and Taucher-Scholz 2004), the above method provides only an estimate of the probabilities. However, the general tendency, that is the significant difference between multiple-hit probabilities in case of uniform and inhomogeneous deposition scenarios, is valid for a modified cell cycle time, as well. If pertinent information on the cell cycle shortening is available, the corresponding multiple-hit probabilities can be easily determined from the lower panel of Fig. 11. This panel depicts the probability of multiple hits as a function of time at a given level of exposure (0.4 WL). The probability of multiple hits in the

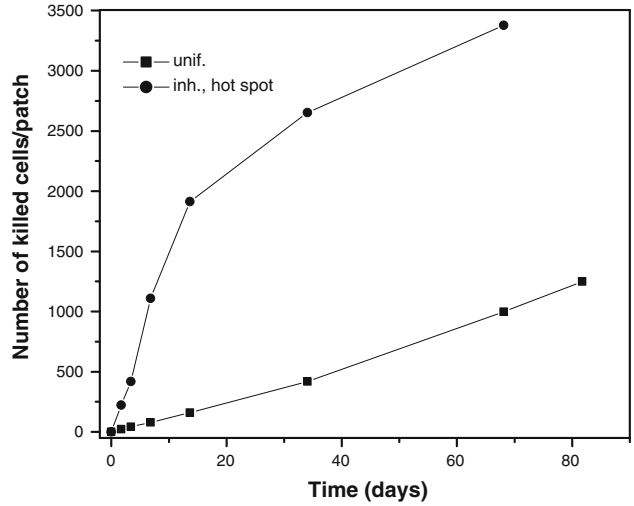

Fig. 12 Number of killed cells per patch as a function of time for uniform radionuclide deposition, and in the deposition hot spot of the inhomogeneous deposition pattern at an exposure level of 0.5 WL, characteristic of Czech uranium mines

highest exposed areas of the bronchial airways within the marked characteristic time periods, e.g. repair halftime (Foray et al. 2005) or one day (Nikjoo et al. 1998), is significantly higher than the same probability assuming uniform activity along the airways.

It is a current paradigm that only high doses can cause deterministic effects. According to ICRP103 (2007), deterministic effects are considered to be the consequence of radiation-induced cell killing (except the case of lens opacity) and the resulting depletion of the tissue. This requires that a critical amount of cells in a given tissue is damaged. Although it is difficult to determine the exact number of the damaged cells needed to produce a deterministic effect, current results seem to challenge this paradigm to some extent. For instance, Fig. 9 demonstrates that even at an exposure level as low as 0.5 WLM in the most exposed area of a bronchial bifurcation, more than 10% of the cells can die due to the emitted alpha particles. According to our computations, 0.5 WLM corresponds to an effective dose of 2.5 mSv. At higher doses, but still below the low-dose threshold, the fraction of killed cells is even higher, leading to extensive tissue damage. Nevertheless, all these cells do not get killed at the same time, and knowledge of the time distribution of cell inactivating events may play a major role in elucidating related health effects.

Figure 12 presents the number of killed cells on a randomly selected surface element for uniformly distributed activity and on the most exposed patch of a realistic deposition pattern as a function of exposure time at 0.5 WL for the same number of deposition events. It can be seen that at the locations characterized by the highest burden, the fraction of inactivated cells can reach 10% within days,

and it can exceed 20% during a normal cell cycle time, while the killing rate characterizing the uniform activity pattern is consistently much lower. The curve characterizing cell killing in the deposition hot spot exhibits some kind of saturation. This is due to the increasing number of multiple hits over time, as the probability of killing individual cells also saturates with the increasing number of hits. Since cell division is not modelled in the present study, the hits received after the cell cycle time also contribute to the number of hits a cell receives, and consequently to the probability of cell death. In addition, cell cycle time itself can be modified by the previous hits and also by the hits received by the neighbouring cells. Because these aspects are not considered in the present approach, the results may be a bit different in a real case. However, the figure shows the general tendencies and the conclusion that even low effective doses can cause extensive local damage remains valid.

As the right panels of Fig. 9 demonstrate, more transformed cells can appear in the deposition hot spot, that is, in the most exposed computational patch, even at low exposure levels. It is known from radiation biology that cancer can develop from a single transformed cell, although transformed cells do not necessarily lead to cancer. However, an increase in the number of "simultaneously" transformed cells relatively close to each other may increase the probability of cancer occurrence. From this point of view, the time between two successive transformation events on the same selected surface element (patch) may be an important parameter.

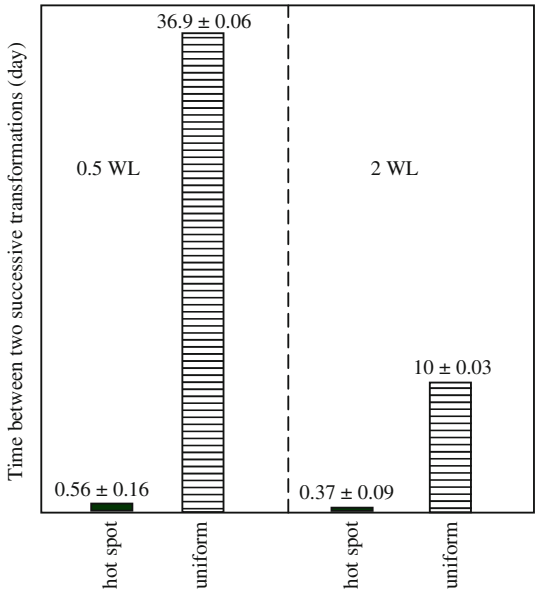

Fig. 13 Time interval between two successive transformation events for a patch with uniform deposition, and for the most exposed patch of non-uniform deposition at two different exposure levels (WL)

In Fig. 13, these time interval values are shown for an arbitrary surface element (with an area equal to 0.43 mm^2) in case of uniform deposition and for the hot spot of the non-uniform deposition pattern at two different working levels. According to the figure for the lower working level (0.5 WL), only about half a day is necessary for two successive transformations on the same patch in the deposition hot spot. Regarding uniform deposition, almost 37 days must elapse in order to have two transformations on the same patch. The corresponding numbers at 2 WL are 0.37 and 10 days, respectively.

Figures 11, 12 and 13 demonstrate that radiobiological events can be highly concentrated not only in space, but also in time. Most probably, computational modelling alone will not give an answer to the question: What is the difference, in terms of biological effects, between having small areas with frequent hits combined with large surfaces with hardly any hit, and rare but uniformly distributed hits? However, accurate simulations can predict time and space distributions of the hits and other radiation related events, which may serve as inputs for further biological experiments focusing on the elucidation of radiation health effects.

Time distributions of the events simulated above can provide useful input data for models of non-targeted effects as well. Cell irradiation experiments revealed that besides the immediate responses of bystander cells, it is possible that cells which display the damage, although derived from the directly irradiated cells, are separated temporally from the initiating event (delayed effects, e.g. genomic instability). These delayed effects and the immediate responses of bystander cells may be propagated by the same or by overlapping signalling pathways and may be different manifestations of the same event (Morgan 2003). Regardless of the underlying mechanisms, which will most probably be elucidated in the future, knowledge of time distributions of cellular/cell nucleus hits, like the ones simulated in the present study, will play an important role in predicting the biological outcome.

Conclusions

In the present study, spatial and temporal distributions of microdosimetric parameters and related biological endpoints in the central bronchial airways were determined by complex computational methods. As expected, the deposition patterns of the inhaled attached and unattached radon progenies are non-uniform within an airway bifurcation with distinct activity hot spots located at the dividing spur (carinal ridge). Cell nucleus hits of radon progeny alpha particles were also heterogeneous in space, although to a slightly lower extent than the distribution of the deposited

radionuclides. The probabilities of single and multiple hits were quite high in the deposition hot spot even at low doses and increased in a non-linear manner with increasing exposure level. The mean distances between hit nuclei were significantly reduced for hot spots compared to the corresponding mean distances in case of uniform deposition. It is worth mentioning that densely ionizing radiation produces a unique type of damage in which multiple lesions are encountered within close spatial proximity. The degree of damage cluster formation can be further enhanced by the non-uniform activity distributions. This feature has been highlighted by the computation of spatial distributions of cell killing and cell transformation. The present computations revealed that high cell killing rates in the deposition hot spot can be observed even at low macroscopic doses. Oncogenic transformation probabilities are also significantly higher at the carinal ridge where transformed cells are closer to each other. Regarding time distributions, the probability of multiple hits in case of a uniform surface activity is low and the hits are well separated in time, while it may be quite high for the cell nuclei located in the deposition hot spot even at low doses. Cell killing arises very frequently in the carinal region and less often elsewhere. Transformations occur relatively frequently in the deposition hot spots, but are quite rare outside of them. By modelling intercellular-induced apoptosis, it could be demonstrated that the deposited radionuclide distribution along the airways may have significant consequences concerning non-targeted effects as well. Present results may help in the elucidation of different aspects concerning the biological consequences of radionuclide inhalation and may serve as inputs for risk assessment models.

Acknowledgments This work has been supported by the European Commission under contract FI6R-CT-2003-508842 (RISC-RAD) and by the Hungarian OTKA K61193 and ETT 317-08 projects.

References

Adamson IYR (1985) Cellular kinetics of the lung. Toxicology of inhaled materials. Springer, Berlin

Balásházy I, Hofmann W, Heistracher T (1999) Computation of local enhancement factors for the quantification of particle deposition patterns in airway bifurcations. J Aerosol Sci 30:185–203

Balásházy I, Hofmann W, Heistracher T (2003) Local particle deposition patterns may play a key role in the development of lung cancer. J Appl Physiol 94:1719–1725

Ballarini F, Alloni D, Facoetti A, Mairani A, Nano R, Ottolenghi A (2006) Modelling radiation-induced bystander effect and cellular communication. Radiat Prot Dosim 122:244–255

Bauer G (2007) Low dose radiation and intercellular induction of apoptosis: potential implications for the control of oncogenesis. Int J Radiat Biol 83:873–888

BEIR VI Report (1999) Health effects of exposure to radon. National Academy Press, Washington, DC

BEIR VII Report (2006) Health risks from exposure to low levels of ionizing radiation. National Academy Press, Washington, DC

Belyakov OV, Mitchell SA, Parikh D, Randers-Pehrson G, Marino SA, Amundson SA, Geard CR, Brenner DJ (2005) Biological effects in unirradiated human tissue induced by radiation damage up to 1 mm away. Proc Natl Acad Sci USA 102:14203–14208

Belyakov OV, Folkard M, Mothersill C, Prise KM, Michael BD (2006) Bystander-induced differentiation: a major response to targeted irradiation of a urothelial explant model. Mutation Res 597:43–49

Böhm B, Nikodémová D, Holy K (2003) Use of various microdosimetric models for the prediction of radon induced damage in human lungs. Rad Prot Dosim 104:127–137

Bowler DA, Moore SR, Macdonald DA, Smyth SH, Clapham P, Kadhim MA (2006) Bystander mediated genomic instability after high LET radiation in murine primary haemopoietic stem cells. Mutation Res 579:50–61

Brenner DJ, Little JB, Sachs RK (2001) The bystander effect in radiation oncogenesis: II. A quantitative model. Radiat Res 155:402–408

Caswell RS, Coyne JJ (1990) Microdosimetry of radon and radon daughters. Rad Prot Dosim 31:395–398

Chatterjee A, Schaefer HJ (1976) Microdosimetric structure of heavy ion tracks in tissue. Radiat Environ Biophys 13:215–227

Churg A, Vedal S (1996) Carinal and tubular airway particle concentrations in the large airways of non-smokers in the general population: evidence for high particle concentration at airway carinas. Occup Environ Med 53:553–558

Crawford-Brown DJ, Hofmann W (1991) An effect-specific track length model for radiation of intermediate to high LET. Radiat Res 126:162–170

Fakir H, Hofmann W, Aubineau-Laniece I (2006) Modelling the effect of non-uniform radon progeny activities on transformation frequencies in human bronchial airways. Rad Prot Dosim 121:221–235

Fakir H, Hofmann W, Tan WY, Sachs RK (2009) Triggering-response model for radiation-induced bystander effects. Radiat Res 171:320–331

Farkas Á, Balásházy I (2007) Simulation of the effect of local obstructions and blockage on airflow and aerosol deposition in central human airways. J Aerosol Sci 38:865–884

Farkas Á, Balásházy I (2008) Quantification of particle deposition in asymmetrical tracheobronchial model geometry. Comp Biol Med 38:508–518

Farkas Á, Balásházy I, Szőcs K (2006) Characterization of regional and local deposition of inhaled aerosol drugs in the respiratory system by computational fluid and particle dynamics methods. J Aerosol Med 19:329–343

Farkas Á, Hofmann W, Balásházy I, Szőke I (2007) CFD as a tool in risk assessment of inhaled radon progenies. Rad Prot Dosim 122:537–539

Fluent User's Guide (2001) Fluent Inc, Lebanon

Foray N, Charvet A-M, Duchemin D, Favaudon V, Lavalette D (2005) The repair rate of radiation-induced DNA damage: a stochastic interpretation based on the Gamma function. J Theor Biol 236:448–458

Ford JR, Terzaghi-Howe M (1993) Effects of ^{210}Po particles on survival and preneoplastic transformation of primary rat tracheal epithelial cells irradiated while in suspension or in the intact tissue. Radiat Res 136:89–96

Fournier C, Taucher-Scholz G (2004) Radiation induced cell cycle arrest: an overview of specific effects following high-LET exposure. Radiother Oncol 73:S119–S122

Gaillard S, Pusset D, Toledo SM, Fromm M, Azzam EI (2009) Propagation distance of α-particle-induced bystander effect: the

role of nuclear traversal and gap junction communication. Radiat Res 171:513–520

Hall EJ, Giaccia AJ (2006) Radiobiology for radiologists, 6th edn. Lippincott Williams & Wilkins, Philadelphia

Harley NH, Chittaporn P (1996) Biological model for lung cancer risk from ^{222}Rn exposure. Environ Int 22:S977–S984

Hegedűs CsJ, Balásházy I, Farkas Á (2004) Detailed mathematical description of the geometry of airway bifurcations. Resp Physiol Neurobiol 141:99–114

Heidenreich WF, Atkinson M, Paretzke HG (2001) Radiation-induced cell inactivation can increase the cancer risk. Radiat Res 155:870–872

Hofmann W, Heistracher T (1996) Track structure predictions of radon-induced biological effects in human bronchial epithelium. Environ Int 22:949–957

Hofmann W, Koblinger L (1990) Monte Carlo modeling of aerosol deposition in human lungs. Part II: deposition fractions and their sensitivity to parameter variations. J Aerosol Sci 21:675–688

Hofmann W, Ménache MG, Crawford-Brown DJ, Caswell RS, Karam LR (2000) Modelling energy deposition and cellular radiation effects in human bronchial epithelium by radon progeny alpha particles. Health Phys 78:377–393

Hofmann W, Asgharian B, Winkler-Heil R (2002) Modeling inter-subject variability of particle deposition in human lungs. J Aerosol Sci 33:219–235

Hofmann W, Winkler-Heil R, Bálásházy I (2006) The effect of morphological variability on surface deposition densities of inhaled particles in human bronchial and acinar airways. Inhal Toxicol 18:809–819

Hui TE, Poston JW, Fisher DR (1990) The microdosimetry of radon decay products in the respiratory tract. Radiat Prot Dosim 31:405–411

ICRP Publication 66 (1994) Human respiratory tract model for radiological protection. Ann ICRP 24

ICRP Publication 103 (2007) The 2007 recommendations of the International Commission on Radiological Protection. Ann ICRP 103

Ina Y, Tanooka H, Yamada T, Sakai K (2005) Suppression of thymic lymphoma induction by life-long low-dose-rate irradiation accompanied by immune activation in C57BL/6 mice. Radiat Res 163:153–158

International Commission on Radiation Units (ICRU) (1993) Stopping powers and ranges for proton and alpha particles. ICRU Report 49. International Commission on Radiation on Radiation Units and Measurements, Inc., Bethesda

Iyer R, Lehnert BE (2000) Factors underlying the cell growth-related bystander responses to α particles. Cancer Res 60:1290–1298

James AC, Birchall A, Akabani G (2004) Comparative dosimetry of BEIR VI revisited. Radiat Prot Dosim 108:3–26

Johnson NF (1995) Radiobiology of lung target cells. Rad Prot Dosim 60:327–330

Jovanovic B, Nikezic D (2010) Probability of bystander effect induced by alpha-particles emitted by radon progeny using the analytical model of tracheobronchial tree. Radiat Prot Dosim 142:168–173

Katz R, Hofmann W (1982) Biological effects of low doses of ionising radiations: particle tracks in radiobiology. Nucl Instrum Meth 203:433–442

Koblinger L, Hofmann W (1985) Analysis of human lung morphometric data for stochastic aerosol deposition calculations. Phys Med Biol 30:541–556

Koblinger L, Hofmann W (1990) Monte Carlo modeling of aerosol deposition in human lungs. Part I: simulation of particle transport in a stochastic lung structure. J Aerosol Sci 21:661–674

Kotin P, Falk HL (1959) The role and action of environmental agents in the pathogenesis of lung cancer. I. Air pollution. Cancer 12:147–163

Kugel C, Bailly I, Tourdes F, Poncy JL (2002) In vitro radiation effects on rat tracheal epithelial cells. I. Different radiosensitivity of cell inactivation after α and γ irradiations. J Radiat Res 43:27–34

Leonard BE (2009) The range of the bystander effect signal in three-dimensional tissue and estimation of the range in human tissue at low radon levels. Radiat Res 171:374–378

Little MP, Wakeford R (2002) The bystander effect in experimental systems and compatibility with radon-induced lung cancer in humans. J Radiol Prot 22:A27–A31

Lorimore SA, Kadhim MA, Pocock DA, Papworth D, Stevens DL, Goodhead DT, Wright EG (1998) Chromosomal instability in the descendants of unirradiated surviving cells after α-particle irradiation. Proc Natl Acad Sci USA 95:5730–5733

Madas BG, Balásházy I, Farkas Á, Szőke I (2010) Cellular burdens and biological effects on tissue level caused by inhaled radon progenies. Radiat Prot Dosim. doi:10.1093/rpd/ncq522

Marples B, Skov KA (1996) Small doses of high-linear energy transfer radiation increase the radioresistance of Chinese Hamster V79 cells to subsequent X radiation. Radiat Res 146:382–387

Marsh JW, Bessa Y, Birchall A, Blanchardon E, Hofmann W, Nosske D, Tomasek L (2008) Dosimetric models used in the alpha-risk project to quantify exposure of uranium miners to radon gas and its progeny. Rad Prot Dosim 130:101–106

Mercer RR, Russel ML, Crapo JD (1991) Radon dosimetry based on the depth distribution of nuclei in human and rat lungs. Health Phys 61:117–131

Mercer RR, Russel RL, Roggli VL, Crapo JD (1994) Cell number and distribution in human and rat airways. Am J Respir Cell Mol Biol 10:613–624

Miller RC, Geard CR, Geard MJ, Hall EJ (1992) Cell-cycle-dependent radiation-induced oncogenic transformation of C3H 10T1/2 cells. Radiat Res 130:129–133

Miller RC, Richard M, Brenner DJ, Hall EJ, Jostes R, Hui TE, Brooks AL (1996) Comparison of oncogenic transformation by accelerator produced monoenergetic alpha particles and by polyenergetic alpha particles from radon progeny. Radiat Res 146:75–80

Miller RC, Randers-Pehrson G, Geard CR, Hall EJ, Brenner DJ (1999) The oncogenic transforming potential of the passage of single a particles through mammalian cell nuclei. Proc Natl Acad Sci USA 96:19–22

Mitchel REJ, Jackson JS, Carlisle SM (2004) Upper dose thresholds for radiation-induced adaptive response against cancer in high-dose-exposed, cancer-prone, radiation-sensitive *Trp53* heterozygous mice. Radiat Res 162:20–30

Mitchell SA, Randers-Pehrson G, Brenner DJ, Hall EJ (2002) The bystander response in C3H 10T1/2 cells: the influence of cell-to-cell contact. Radiat Res 161:397–401

Morgan WF (2003) Non-targeted and delayed effects of exposure to ionizing radiation: I. Radiation induced genomic instability and bystander effects in vitro. Radiat Res 159:567–580

National Research Council (NRC) (1991) Comparative dosimetry of radon in mines and homes. National Academy Press, Washington DC

Nikezic D, Yu KN (2001) Alpha hit frequency due to radon decay products in human lung cells. Int J Radiat Biol 77:559–565

Nikezic D, Haque AKMM, Yu KN (2002) Absorbed dose delivered by alpha particles calculated in cylindrical geometry. J Environ Radioact 60:293–305

Nikjoo H, Khvostunov IK (2003) Biophysical model of radiation-induced bystander effect. Int J Radiat Biol 79:43–52

Nikjoo H, Uehara S, Wilson WE, Moshi M, Goodhead DT (1998) Track structure in radiation biology: theory and applications. Int J Radiat Biol 73:355–364

Portess D, Bauer G, Hill MA, O'Neill P (2007) Low-dose irradiation of nontransformed cells stimulates the selective removal of precancerous cells via intercellular induction of apoptosis. Cancer Res 67:1246–1253

Puck TT, Steffen J (1963) Life cycle analysis of mammalian cells. I. A method for localizing metabolic events within the life cycle, and its application to the action of colcemide and sublethal doses of X-irradiation. Biophys J 3:379–397

Robbins ES, Meyers OA, Harley NH (1990) Quantification of the nuclei of human bronchial epithelial cells from electron micrographs for radon risk analysis. In: Proceedings of the XIIth international congress for electron microscopy, San Francisco Press, San Francisco, CA

Ruzer LS, Nero AV, Harley NH (1995) Assessment of lung deposition and breathing rate of underground miners in Tadjikistan. Radiat Prot Dosim 58:261–268

Saccomanno G, Auerbach O, Kuschner M, Harley NH, Michels RY, Anderson MW, Bechtel JJ (1996) A comparison between the localization of lung tumors in uranium miners and nonminers from 1974 to 1991. Cancer 77:1278–1283

Sawant SG, Randers-Pehrson G, Geard CR, Brenner DJ, Hall EJ (2001a) The bystander effect in radiation oncogenesis: I. Transformation in C3H 10T1/2 cells in vitro can be initiated in the unirradiated neighbours of irradiated cells. Radiat Res 155:397–401

Sawant SG, Randers-Pehrson G, Metting MF, Hall EJ (2001b) Adaptive response and bystander effect induced by radiation in C3H 10T1/2 cells in culture. Radiat Res 156:177–180

Schettino G, Folkard M, Michael BD, Prise KM (2005) Low dose binary behavior of bystander cell killing after microbeam irradiation of a single cell with focused C_K X rays. Radiat Res 163:332–336

Sedlák A (1996) Microdosimetric approach to the problem of lung cancer induced by radon progenies. Health Phys 70:680–688

Shao C, Folkard M, Michael BD, Prise KM (2004) Targeted cytoplasmic irradiation induces bystander effects. Proc Natl Acad Sci USA 37:13495–13500

Shuryak I, Sachs RK, Brenner DJ (2007) Biophysical models of radiation bystander effects: 1. Spatial effects in three-dimensional tissues. Radiat Res 168:741–749

Simmons JA, Cohn P, Min T (1996) Survival and yields of chromosome aberrations in hamster and human lung cells irradiated by alpha particles. Radiat Res 145:174–180

Sutherland JC (2006) Repair dependent radiation survival: a stochastic model with Euler gamma functions. Phys Med Biol 51:4883–4901

Szőke I, Farkas Á, Balásházy I, Hofmann W (2008) Modelling of cell deaths and cell transformations of inhaled radon in homes and mines based on a biophysical and microdosimetric model. Int J Rad Biol 84:127–138

Tapio S, Jacob V (2007) Radioadaptive response revisited. Radiat Environ Biophys 46:1–12

Thomassen DG, Seiler FA, Shyr LJ, Griffith WC (1990) Alpha-particles induce preneoplastic transformation of rat tracheal epithelial cells in culture. Int J Radiat Biol 57:397–405

Tomasek L, Rogel A, Tirmarche M, Mitton M, Laurier D (2008) Lung cancer in French and Czech uranium miners: radon associated risk at low exposure rates and modifying effects of time since exposure and age at exposure. Radiat Res 169:125–137

Truta-Popa LA, Hofmann W, Fakir H, Cosma C (2008) Biology based lung cancer model for chronic low radon exposures. AIP Conf Proc 1034:78–85

Veeze P (1968) Rationale and methods of early detection in lung cancer. van Gorcum, Assen

Wingate CL, Baum JW (1976) Measured radial distributions of dose and LET for alpha and proton beams in hydrogen and tissue-equivalent gas. Radiat Res 65:1–19

Wu LJ, Randers-Pehrson G, Xu A, Waldren CA, Geard CR, Yu Z, Hei TK (1999) Targeted cytoplasmic irradiation with alpha particles induces mutations in mammalian cells. Proc Natl Acad Sci USA 96:4959–4964

Yarbro CH, Frogge MH, Goodman M (2005) Cancer nursing, principles and practice, 6th edn. Jones and Bartlett Publishers, Sudburry

Zhou H, Randers-Pehrson G, Waldren CA, Vannais D, Hall EJ, Hei TK (2000) Induction of bystander mutagenic effect of alpha particles in mammalian cells. Proc Natl Acad Sci USA 97:2099–2104